Delay Time Distributions of Type Ia Supernovae From Galaxy and Cosmic Star Formation Histories

Louis-Gregory Strolger,[1] Steven Rodney,[2] Camila Pacifici,[1] Gautham Narayan,[3] and Or Graur[4, 5, 6]

[1]*Space Telescope Science Institute, 3700 San Martin Drive, Baltimore MD 21218, USA*
[2]*University of South Carolina*
[3]*University of Illinois Urbana-Champaign*
[4]*Center for Astrophysics — Harvard & Smithsonian, 60 Garden Street, Cambridge, MA 02138, USA*
[5]*Department of Astrophysics, American Museum of Natural History, Central Park West and 79th Street, New York, NY 10024, USA*
[6]*NSF Astronomy and Astrophysics Postdoctoral Fellow.*

## ABSTRACT

We present analytical reconstructions of type Ia supernova (SN Ia) delay time distributions (DTDs) by way of two independent methods: by a Markov chain Monte Carlo best-fit technique comparing the volumetric SN Ia rate history to today's compendium cosmic star-formation history, and secondly through a maximum likelihood analysis of the star formation rate histories of individual galaxies in the GOODS/CANDELS field, in comparison to their resultant SN Ia yields. We find a family of solutions that are essentially exponential DTDs, similar in shape to the $\beta \approx -1$ power-law DTDs, but with more delayed events ($> 1$ Gyr in age) than prompt events ($< 1$ Gyr). These solutions have the additional benefit of being consistent with empirically recovered delay time measures, without requiring different power-law slopes for events in field and galaxy cluster environments. These models are generally inconsistent with results from single-degenerate binary populations synthesis models, and seemingly supportive of double-degenerate progenitors for most SN Ia events.

## 1. INTRODUCTION

The understanding of cosmic type Ia supernova (SN Ia) rates has critical importance to understanding galaxy evolutionary feedback mechanisms, cosmic iron enrichment and $\alpha$-process element enrichment histories (see Maoz & Graur 2017), and perhaps most importantly, constraining the physical mechanisms of SN Ia progenitors, and therefore providing some constraint on the systematic uncertainties of dark energy. However, determining precise SN Ia rates and rate histories, and establishing the connections of those rates to host (and cosmic) properties has been a long slog.

In tracing the cosmic (or volumetric) rate history, the first precise measures of the local ($z \sim 0$) rate came in the early 1990s (cf. Cappellaro et al. 1993; Cappellaro et al. 1999), and the first measures beyond the local Hubble flow came in the early 2000s, many as collateral results of dark energy experiments (Riess et al. 1998; Perlmutter et al. 1999). This trend of collateral benefit has continued since, leading to a vast collection of volumetric rates over various redshift ranges, and from various groups, as shown in Figure 1 (the individual measures are shown in Appendix A).

Not all rate measures have been in agreement with one another (see the large scatter just below $z \sim 0.5$), with the reasons as to why ranging from statistical variation, differences in the treatment of declining SNe, and ultimately differences in the assessment of effective survey duration, via modeling and simulation. It is left to a future study to attempt a reanalysis of some (or all) of the reported rate measures in at least a self-consistent assessment to reduce some of the unreported systematic uncertainties. For the time being, it is probably best to consider each published rate as a valid measure that may (or may not) have misestimated uncertainties.

From this rate history and a comparison to the cosmic star formation history, one can reconstruct (or infer) the distribution of times from SN progenitor formation to explosion, assuming the mechanism is ubiquitous enough that it can be characterized by a singular distribution of delay times. It has been long expected that this 'delay time distribution' (or DTD) will distinguish between single-degenerate (Whelan & Iben 1973; Nomoto 1982) and double-

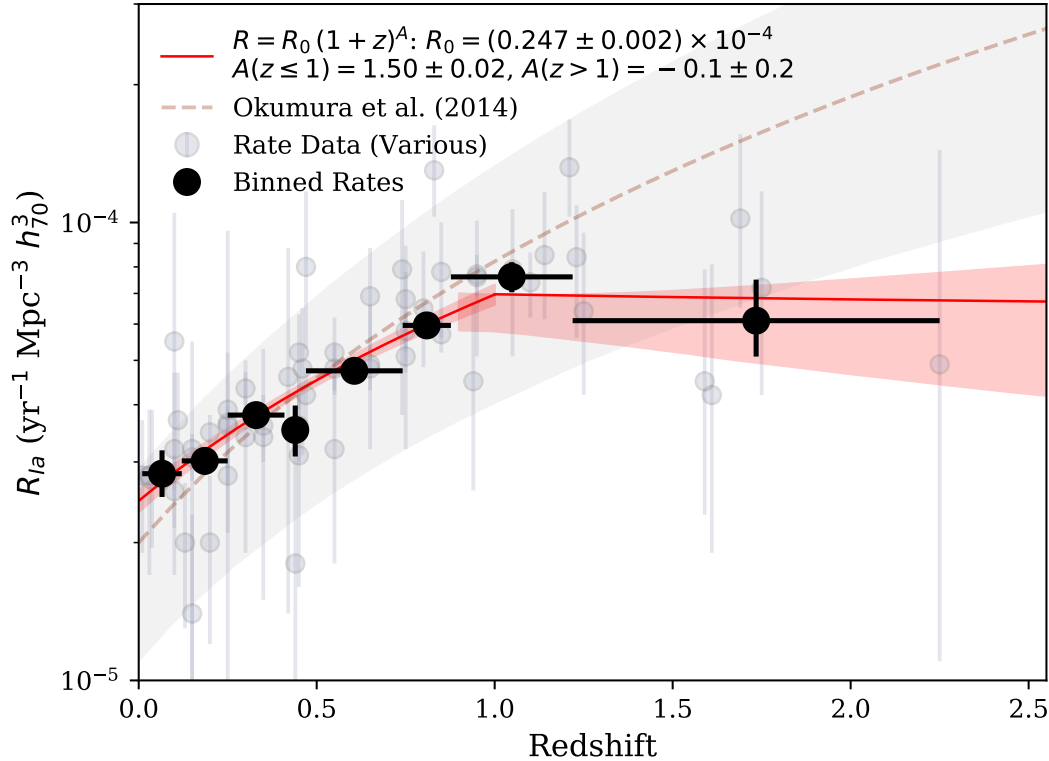Corresponding author: Lou Strolger
strolger@stsci.edu

**Figure 1.** Type Ia supernova volumetric rate measures from various sources in the literature (gray points, see Table A for their sources), and binned (black points, see Table 1), largely for illustration. The solid red lines show a broken power-law fit to the data in redshift space. The dashed red line (and associated uncertainty region, in gray) is from Okumura et al. (2014).

degenerate (Iben & Tutukov 1984; Webbink 1984) models, depending on what the models for each of these scenarios would expect (see Section 2.3 for more details).

Another method in reconstructing delay times results from an analysis of the star-formation histories in individual host galaxies (Brandt et al. 2010; Maoz et al. 2011, 2012), under the same assumptions as above. Rather than using bulk star formation properties, averaged in large temporal bins (or by redshift), the method uses spectral analysis tools to reconstruct star formation histories, then determine the contributions (over broad periods or time bins) from a DTD that maximizes the likelihood that the hosts would produce SNe Ia in the duration of a survey. The results of which, to date, are (A) dependent on the presumed power-law shape of the DTD model, (B) have different power-law slopes in galaxy cluster and field environments, independent of redshift, and (C) have not been tested on high-$z$ ($z \gtrsim 1$) field galaxies.

In this paper, we present an analysis of DTDs using these two separate methods, from a comparison of volumetric SN Ia rates to cosmic star formation rates (Section 2), and a maximized likelihood method from SN Ia host star formation histories (Section 3). In Section 4 we discuss the results from each of these methods and put them into context with results from other work, and into context with binary synthesis models. Throughout this manuscript we assume $H_0 = 70$ km s$^{-1}$ Mpc$^{-3}$, $\Omega_M = 0.27$ and $\Omega_\Lambda = 0.73$.

## 2. DELAY TIME DISTRIBUTIONS FROM VOLUMETRIC SN IA RATES AND THE COSMIC STAR FORMATION HISTORY

The various SN Ia volumetric rate measurements are shown in Table A and Figure 1. For illustration purposes only, here and throughout this manuscript, we bin the rate data into 8 quantiles of nearly equal number of measures and present those binned measures, weighted by reported statistical uncertainties only, in Figure 1 and in Table 1. None

of the analysis presented herein was performed directly on the binned measures, rather on the individual rate values themselves.

**Table 1.** Binned volumetric SN Ia rates, with statistical uncertainties.

| Redshift | $R_{\mathrm{Ia}}$[a] | $N_{\mathrm{measures}}$ |
|---|---|---|
| $0.07 \pm 0.06$ | $0.28^{+0.04}_{-0.03}$ | 7 |
| $0.19 \pm 0.06$ | $0.30^{+0.02}_{-0.02}$ | 6 |
| $0.33 \pm 0.08$ | $0.38^{+0.02}_{-0.02}$ | 8 |
| $0.44 \pm 0.03$ | $0.35^{+0.05}_{-0.04}$ | 6 |
| $0.61 \pm 0.14$ | $0.47^{+0.03}_{-0.03}$ | 9 |
| $0.81 \pm 0.07$ | $0.60^{+0.04}_{-0.04}$ | 7 |
| $1.05 \pm 0.17$ | $0.76^{+0.06}_{-0.06}$ | 7 |
| $1.73 \pm 0.52$ | $0.61^{+0.14}_{-0.10}$ | 7 |

[a]In units of $10^{-4}$ yr$^{-1}$ Mpc$^{-3}$ $h_{70}^3$

A conveniently simple empirical model for volumetric rate evolution with redshift is a broken power law evolution with redshift, $R_{\mathrm{Ia}} = R_0 (1+z)^A$. As shown in Figure 1, fixing the redshift break at $z = 1$ (arbitrarily) and performing a least-squares fit would give a power-law slope at $z < 1$ is $A = 1.50 \pm 0.02$ (with $R_0 = 2.47 \pm 0.02 \times 10^{-5}$ yr$^{-1}$ Mpc$^{-3}$ $h_{70}^3$), which then flattens substantially to $A = -0.1 \pm 0.2$ at redshifts greater than 1. This is broadly consistent with the power-law fit from Okumura et al. (2014), especially to $z \lesssim 1$. The locus is also consistent with the volumetric SN Ia rate at $z \approx 0$ converted by Li et al. (2011) to $2.7 \pm 0.3 \times 10^{-5}$ yr$^{-1}$ Mpc$^{-3}$ $h_{70}^3$. While the broken power-law model is useful for predicting yields from volumetric surveys, e.g., for the Wide Field InfraRed Survey Telescope (*WFIRST*, Hounsell et al. 2018) and the Large Synoptics Survey Telescope (*LSST*, Kessler et al. 2019), it does not inherently reveal much on the nature of SN Ia progenitor mechanisms, which is better done through an assessment of delay-time distributions.

For these types of analyses, the standard assumption is that the stellar death rate (or supernova rate) is related to the stellar birth rate, convolved with some DTD that contains all the temporal factors of stellar evolution (e.g., main sequence lifetime, etc.) and binary star evolution (e.g., accretion rates or merger times). Two additional factors could include the fraction of the initial mass function (or IMF) that the progenitors of SNe Ia arise from, presumably $3-8\,\mathrm{M}_\odot$ zero-age main sequence stars (as discussed in Section 2.1) and the fraction of that population that are actually capable of producing events, as not all progenitor stars are necessarily in binary systems, or presumably the right type of binary systems to successfully result in SNe Ia.

We can relate volumetric SN Ia rate history to the cosmic star formation history($\dot{\rho}_\star$) in a similar way, expressed mathematically by,

$$R_{\mathrm{Ia}}(t) = h^2 \, k \, \varepsilon \left[ \dot{\rho}_\star(t) * \Phi(t) \right], \tag{1}$$

where $\Phi(t)$ is the DTD, $k$ is the fraction of the IMF (by mass) responsible for SN Ia progenitors, $\varepsilon$ is the fraction of that population that are ultimately successful in producing SNe Ia, and $t$ is the forward-moving clock of the universe. The two factors of the dimensionless Hubble constant ($h$) arise from the determination of stellar mass formation from luminosity in $\dot{\rho}_\star(t)$ (see Croton 2013).

## 2.1. *The Fraction of Stars Responsible for SNe Ia*

Dissecting each of the terms in Equation 1, $k$ is perhaps the easiest to approximate. The progenitors of SNe Ia have traditionally been CO WD which acquire sufficient mass to approach or exceed the Chandrasekhar mass limit, $M_{ch} = 1.44\,M_\odot$. To only marginally achieve this, they can either start at sufficiently high mass to require only a small amount of accretion from a nearby companion (typically single-degenerate, or SD, scenarios), or as a pair of WD that have combined in mass to meet this criterion (the double-degenerate, or DD, scenario) setting an even lower initial constraint (see Maoz et al. 2014, for a review). In the case of DD mergers, WD mass distributions are strongly peaked around $M_{\mathrm{WD}} \approx 0.6 \pm 0.1\,M_\odot$ (Catalán et al. 2008), in which a pair drawn from such distribution may be satisfactorily close to the ignition threshold of a carbon core for a non-rotating CO WD, approximately $1.38\,M_\odot$

(Arnett 1969; Nomoto 1982; Pakmor et al. 2013). Initial-Final Mass relations (e.g., Catalán et al. 2008; Cummings et al. 2018) would correspond these to zero-age main-sequence (ZAMS) masses of approximately $3\,M_\odot$, but no less than approximately $2.5\,M_\odot$.

The same Initial-Final Mass relations would suggest that a WD essentially at $M_{ch}$ would fall just below $8\,M_\odot$ ZAMS. Similarly, simulations show that the lowest mass in which C ignition is still possible is around $6 - 8\,M_\odot$ Chen et al. (2014); Denissenkov et al. (2015), but likely no more than $\sim 11\,M_\odot$ (Takahashi et al. 2013), above which an electron-capture-induced collapse mechanism begins, marking the onset of core-collapse supernovae. It is reasonable, therefore, to assume a SN Ia progenitor mass range of about $3 - 8\,M_\odot$ ZAMS.

From a numerical assessment of these stars, assuming they fall within an IMF that is a power-law distribution by mass in this initial mass range, with $\alpha \approx -2.3$ (Salpeter 1955; Kroupa 2001), one would expect

$$k = \frac{\int\limits_{3M_\odot}^{8M_\odot} \xi(M)\,dM}{\int\limits_{0.1M_\odot}^{125M_\odot} M\,\xi(M)\,dM} = 0.021^{+33\%}_{-24\%}\,M_\odot^{-1}, \tag{2}$$

where error in $k$ is driven more by choices in the upper and lower value in the selected mass range of SN Ia progenitors than by the choice in IMF model, as detailed above.

The fraction of CO WDs that are ultimately successful in making SNe Ia is hard to determine, as we do not yet know the details of the progenitor mechanism or mechanisms. Estimates swing rather wildly from (perhaps) as low as 1 in 200 (Breedt et al. 2017) to as optimistic as 1 in 40 (Maoz & Mannucci 2012). There is at least strong consensus that accretion on to a CO WD is essential, but that broadly describes a wide range of very different yet plausible WD close binary scenarios, at least from a theoretical standpoint (Nelemans et al. 2001a,b). The binary fractions of WDs estimated from the ESO-VLT Supernova-Ia Progenitor Survey (SPY; Napiwotzki et al. 2007, 2019) suggest close double WD systems have $\varepsilon_{\rm bin} \simeq 0.1 \pm 0.02$ (Maoz & Hallakoun 2017). It is not likely all of these systems successfully yield SNe Ia as their merger rates in the Milky Way would imply event rates at least a magnitude higher than best estimates of the SN Ia rate in our galaxy, and presumably some of these systems will form AM CVn and R Corona Borealis stars. But at least this estimate could be treated as an upper limit on $\varepsilon$.

### 2.2. *The Star Formation Density History*

The cosmic star formation history (CSFH), at least to $z < 5$ or over 90% of the history of the universe, is fairly well understood, with Madau & Dickinson (2014; MD14 hereafter) providing one of the most complete compilations. More recently, the CSFH derived from the combined GAMA, G10-COSMOS, and 3D-HST datasets by Driver et al. (2018), in a quasi-homogeneous analysis over a larger area, provides a dataset with greatly reduced uncertainties per datum, but fewer data than presented in the MD14 compendium (see Figure 2). We combine the MD14 and Driver et al. (2018) data, with additional star-formation rate densities from Bouwens et al. (2015) and Khusanova et al. (2019), to arrive at today's compendium CSFH using the parameterization,

$$\dot{\rho}_\star(z) = \frac{A\,(1+z)^C}{((1+z)/B)^D + 1}. \tag{3}$$

However to do so, we must also correct the Driver et al. (2018) data for dust attenuation following the prescription in MD14, by applying

$$\dot{\rho}_\star(z) = h^3 \left[ 1 + 10^{0.4 \cdot A_{\rm FUV}(z)} \right] \dot{\rho}_{\star,\rm uncorrected}(z), \tag{4}$$

where it is assumed $A_{\rm FUV}(z)$ has the same functional form of Equation 3, with $A = 1.4 \pm 0.1$, $B = 3.5 \pm 0.4$, $C = 0.7 \pm 0.2$, and $D = 4.3 \pm 0.7$ as determined from the $A_{\rm FUV}(z)$ data from MD14. We then fit Equation 3 to the combined CSFH datasets, resulting in Levenberg-Marquardt least-squares solution parameters which are excellently constrained, as shown in Table 2 and Figure 2.

### 2.3. *SN Ia Progenitor Delay-Time Distribution Models*

Theoretical DTDs result from physically constrained analyses of binary population synthesis (see Wang & Han 2012, for a review). In SD scenarios, details ranging from composition of the companion donor star (H or He) to the
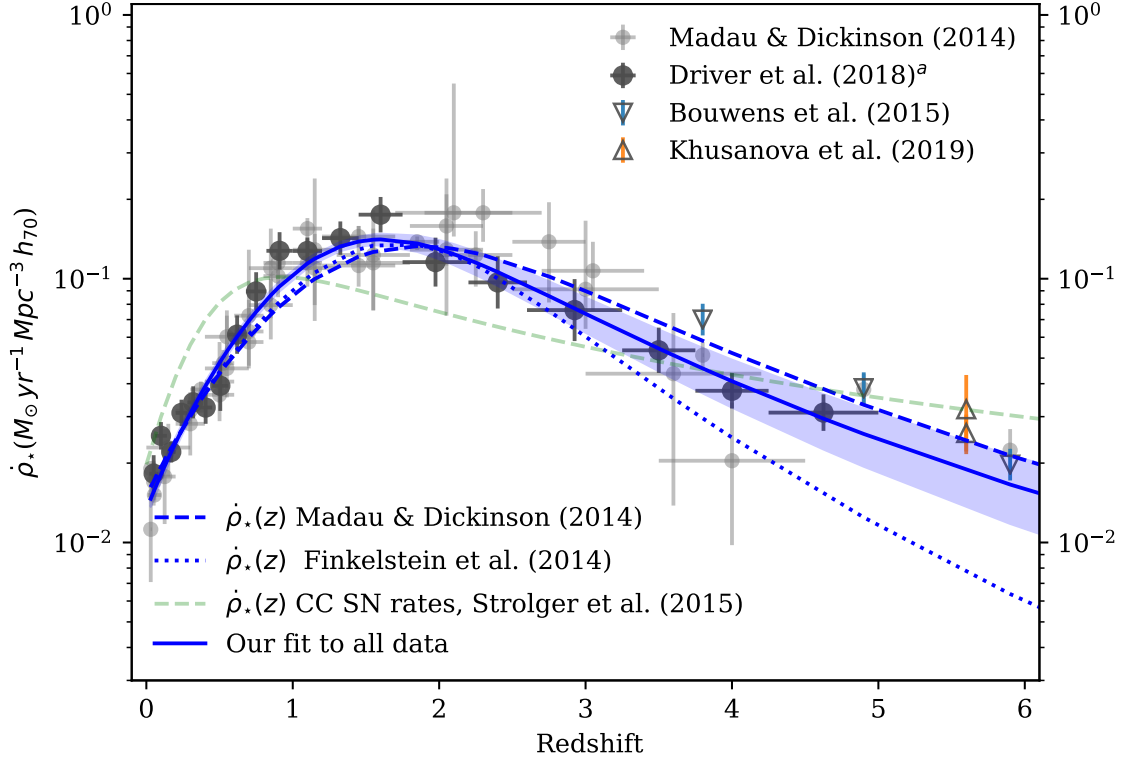
**Figure 2.** Shown are a compendium of cosmic star formation histories measures, from Madau & Dickinson (2014), Driver et al. (2018; [a]-dust corrected), Bouwens et al. (2015), and Khusanova et al. (2019). Dashed and dotted lines are previous models from Madau & Dickinson (2014), Finkelstein et al. (2014), Strolger et al. (2015), as indicated. Solid blue line (and blue shaded region) represent our best-fit model to the compendium of data.

**Table 2.** Cosmic Star Formation History Fit Parameter

|  | $A$ | $B$ | $C$ | $D$ |
|---|---|---|---|---|
| Madau & Dickinson (2014) | 0.015 | 2.9 | 2.7 | 5.6 |
| Finkelstein et al. (2014) | 0.015 | 2.9 | 2.7 | 7.0 |
| Strolger et al. (2015), CCSNe | $0.015 \pm 0.001$ | $1.5 \pm 0.1$ | $5.0 \pm 0.2$ | $6.1 \pm 0.2$ |
| Madau & Dickinson (2014)[a] data fit | $0.013 \pm 0.001$ | $2.6 \pm 0.1$ | $3.2 \pm 0.2$ | $6.1 \pm 0.2$ |
| Driver et al. (2018)[b] data fit | $0.014 \pm 0.001$ | $2.5 \pm 0.2$ | $3.3 \pm 0.3$ | $6.2 \pm 0.3$ |
| Combined Data Fit | $0.0134 \pm 0.0009$ | $2.55 \pm 0.09$ | $3.3 \pm 0.2$ | $6.1 \pm 0.2$ |

[a]New fit to the cited tabular data.

[b]Corrected for dust attenuation.

mass-accretion efficiency lead to rather large variations in the expected DTDs Nelemans et al. (2013). DD models, however, are in reasonable agreement with one another, largely because the scenario is governed by the loss of angular momentum due in the radiation of gravitational waves. The timescales involved depend on the initial separations of the WDs. It is assumed that the population WD binaries follow a power-law of initial radial distributions, $\Phi(r) = r^\beta$, with power $\beta \approx -1$ (Öpik 1924), as is supported by SPY close WD systems, with separations distributed following $\beta = -1.3 \pm 0.2$ (Maoz & Hallakoun 2017). It follows that the resultant delay time distribution will also follow a power-law distribution, $\Phi(t) = t^\beta$, with a power close to $\beta \approx -1$.
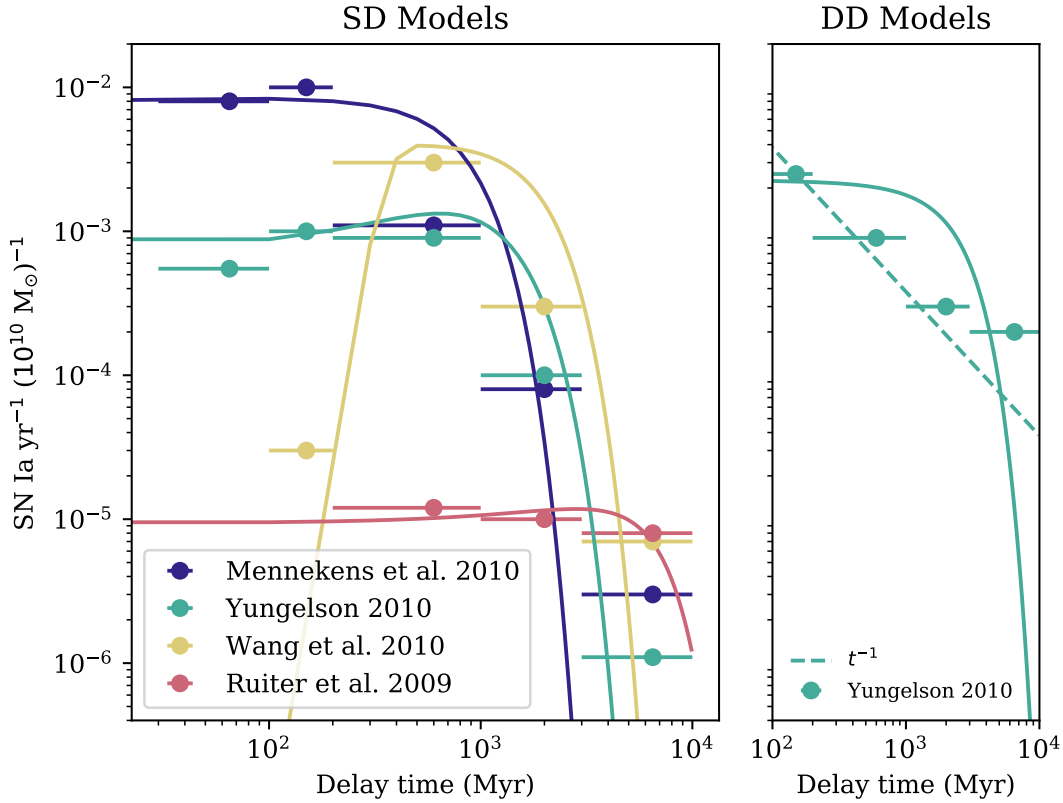
**Figure 3.** Examples of delay-time distributions from binary population synthesis analyses for SD (left) and DD (right) scenarios, from Nelemans et al. (2013). Shown also (as solid line) are fits to these model bins using the function described in Equation 5, tuning dependent variables $\xi$, $\omega$, and $\alpha$. These are the best the function can do at representing these models, if they are indeed preferred by the data.

DTD recovery methods based on matching theoretical $\Phi(t)$ to CSFHs and SN Ia volumetric rates has been hampered largely by the uncertainty in the latter two (Dahlen et al. 2008; Strolger et al. 2010; Graur et al. 2014; Rodney et al. 2014), specifically in the uncertainty in the SN Ia rate above 'SN high noon' (around $z \sim 1$), and the uncertainty in CSFH above 'cosmic high noon' (around $z \sim 2$). It seems now, however, that those uncertainties have reduced to the point of making a $\Phi(t)$ reconstruction viable.

Following the methodology in Strolger et al. (2010), we can test the intrinsic shape of the delay time distribution using a tunable unimodal model, then compare the results to the shapes of the theoretical distributions for SD and DD models. We use a skew-normal $\Phi(t)$ function, defined as:

$$\Phi(t) = \frac{1}{\omega\pi} \exp\left(\frac{-(t-\xi)^2}{2\omega^2}\right) \int_{-\infty}^{\alpha\left(\frac{t-\xi}{\omega}\right)} \exp\left(\frac{-t'^2}{2}\right) dt', \tag{5}$$

where location ($\xi$), width ($\omega^2$), and shape ($\alpha$) are the dependent variables.[1] Figure 3 demonstrates the flexibility of the function in reproducing various model SD and DD from Nelemans et al. (2013). As can be seen, the defined function does a fairly good job of reproducing the shapes of various binary population synthesis models, particularly for SD distributions. It is also fairly reasonable in fitting DD distributions, although it should be emphasized that due to the exponential nature of the function, it has trouble *exactly* reproducing the shape of a distribution that is intrinsically a power-law, a point that will be revisited in Section 4.

---

[1] $\xi$ and $\alpha$ here are different from the initial mass function, $\xi(M)$, and the power-law slope of the initial mass function at the low-mass end, respectively.
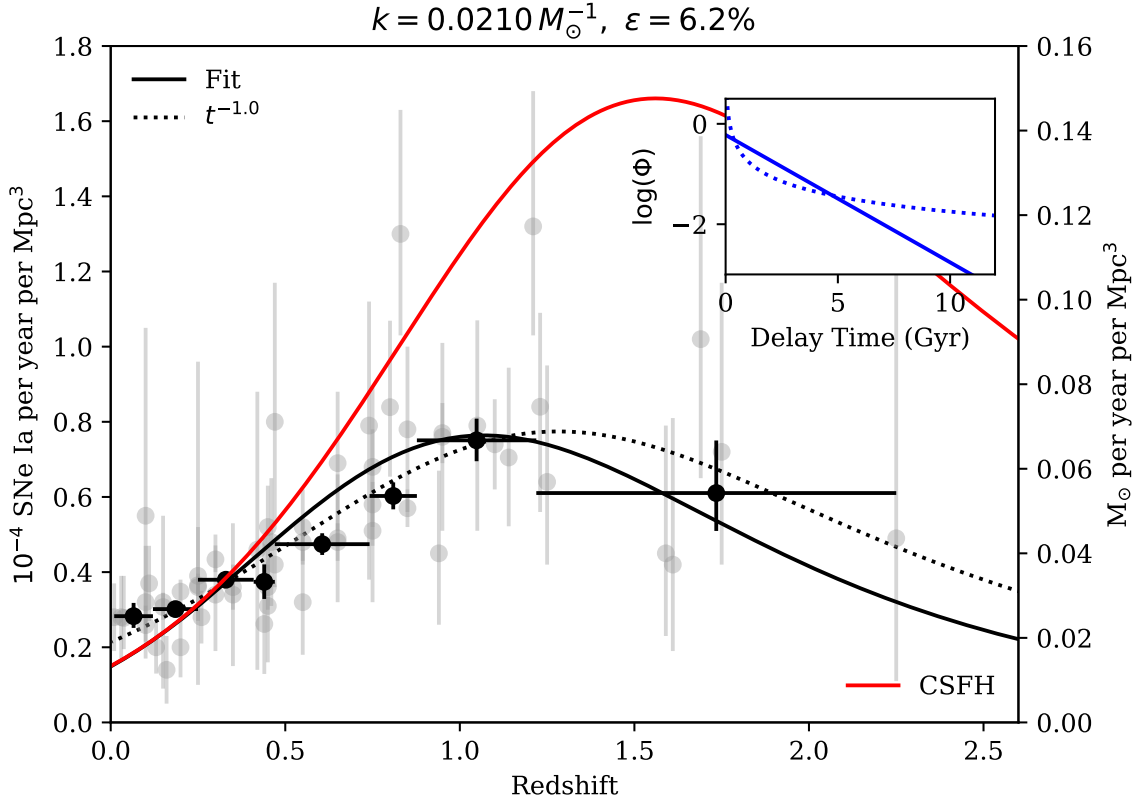
**Figure 4.** In addition to rate values shown in previous figures, the $R_{\rm Ia}(z)$ model results of from optimal parameter fitting of the unimodal $\Phi(\tau)$ model is shown (solid black line) in comparison to a $\beta = -1$ power-law $\Phi(\tau)$ (dashed black line). The inset shows the comparison of the two $\Phi(\tau)$ models. The CSFH is shown on in red, and along the secondary ordinate.

Either through an optimized fit of the functional parameters ($\xi$, $\omega$, and $\alpha$), or through a Markov-chain monte carlo (MCMC), we can test model $\Phi(t)$ through Equation 1 in comparison to the volumetric rate measurements.

### 2.4. *The Optimized Solution*

We apply a maximum likelihood estimation method to determine the best-fit skew normal delay time model to Equation 1 using an optimized method described in Hogg et al. (2010). For simplicity, we assume that the errors of all survey data ($\sigma_i$) are gaussian in nature, but may be underestimated by some factor ($f$), which is justified even if only by the fact that we are using just the statistical error reported for each rate value. As follows, we adopt the likelihood function to be:

$$\ln p(y|x,\sigma,\varepsilon,\xi,\omega,\alpha,f) = -\frac{1}{2}\sum_i \left\{ \frac{[R_{\rm Ia,i} - R_{\rm Ia}(t_i;\varepsilon,\xi,\omega,\alpha)]^2}{s_i^2} + \ln(2\pi s_i^2) \right\}, \tag{6}$$

where,

$$s_i^2 = \sigma_i^2 + f^2 \, R_{\rm Ia}(t_i;\varepsilon,\xi,\omega,\alpha)^2, \tag{7}$$

$R_{\rm Ia,i}$ are the various independent rate measures, and $R_{\rm Ia}(t_i)$ are the parameter-dependent model predictions at the cosmic time of the various rate measures. We then find the optimal parameters which maximize this likelihood.

As for priors, we require the successful fraction of progenitors to be between zero and unity ($0 < \varepsilon < 1$), that the width parameter can only be positive ($\omega > 0$), and that the underestimation fraction can only be between approximately zero and unity ($-4 < \ln f < 0$). Otherwise, we apply rather loose and arbitrary bounds of $-2000 < \xi < 2000$ and $-500 < \alpha < 500$. The results of this optimized fit are shown in Figure 4 and tabulated in Table 3.
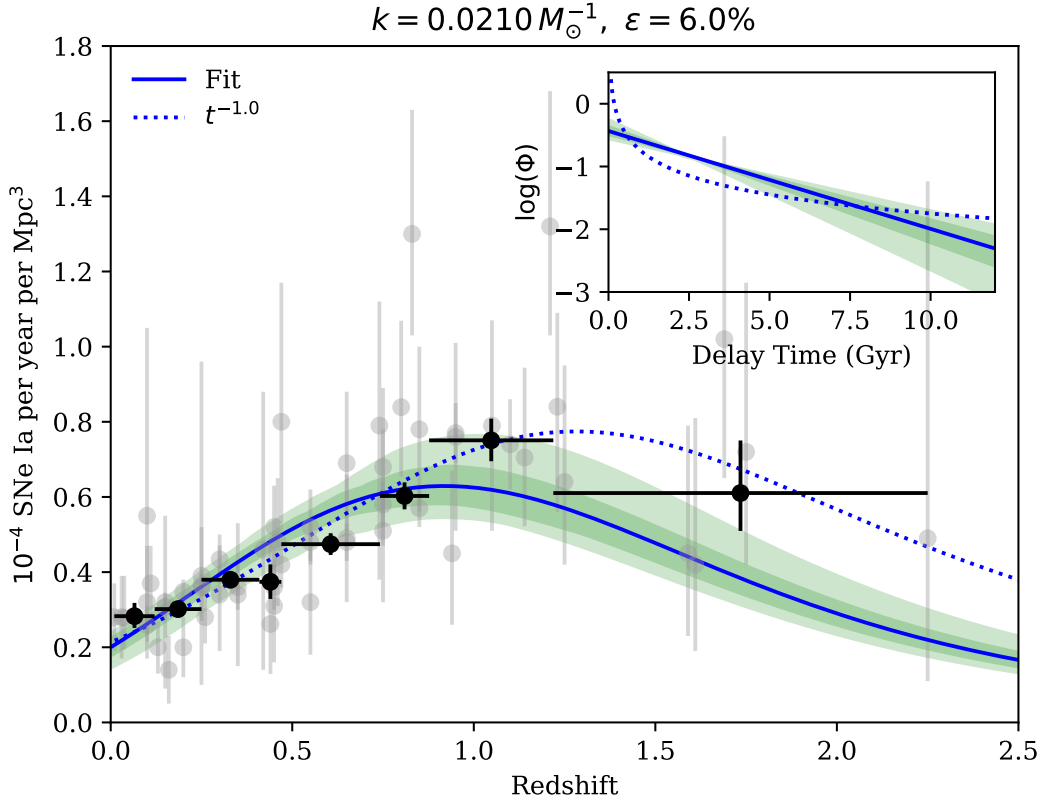
**Figure 5.** Similar to Figure 4, the $R_{\mathrm{Ia}}(z)$ result of from MCMC best-fit is shown (blue line), with the 68% and 95% confidence intevals, in dark and light green, respectively.

The optimization results in a model that is seemingly consistent with the $t^{-1}$ model, although it is not directly possible to estimate errors on the best-fit parameters, or the range of validity via this maximum likelihood optimization method.

**Table 3.** Results for Skew-normal Model fits

| Model test | $\ln \varepsilon$ | $\xi$ | $\omega$ | $\alpha$ | $\ln f$ |
|---|---|---|---|---|---|
| CSFH Max. Likelihood (Optimized) | $-2.78$ | $-1518$ | $51$ | $50$ | $-2.41$ |
| CSFH MCMC | $-2.81^{+0.05}_{-0.05}$ | $-1258^{+523}_{-669}$ | $59^{+18}_{-12}$ | $248^{+169}_{-171}$ | $-2.6^{+0.8}_{-0.7}$ |
| SFH MCMC | $\cdots$ | $-1087^{+561}_{-604}$ | $73^{+22}_{-17}$ | $242^{+168}_{-173}$ | $\cdots$ |

### 2.5. The MCMC solution

Exploring the parameter space in an MCMC allows both confirmation of the optimized solution and an exploration of the range of validity. We use the affine-invariant MCMC ensemble sampler from `emcee.py` (Foreman-Mackey et al. 2013) using the same likelihood function as shown in Equation 6, and set our uniform priors as described by the bounds, as shown in the previous section, with the exception of evaluating $\ln \varepsilon$ rather than $\varepsilon$ to allow MCMC step sizes of order unity, and using the prior $-10 < \ln \varepsilon < 0$. We then set 1,000 walkers to explore 10,000 steps, for a total of 10 million iterations, the first 100,000 of which are discarded as 'burn-in'. The MCMC likelihood distributions are presented in the Appendix B. The median solution and confidence range is shown in Figure 5 and tabulated in Table 3.

As these result show, there is a clear convergence in $f$, the factor by which statistical errors in rate measures are collectively misestimated. We find that $\ln(f) = -2.8^{+0.6}_{-0.8}$, which means that the published rate measures are

collectively underestimated by $\sim 4\%$ to $17\%$. So, while there is a large dispersion in rate values, these values are reasonably consistent to within statistical errors, which themselves are not grossly misestimated. The fraction $\varepsilon$ is also very well constrained, with only $6.0 \pm 0.3\%$ of WD stars contributing as SN Ia progenitors. The Hubble-time integrated SN Ia production efficiency, i.e., combining the $k$ and $\varepsilon$ terms, yields $N/M_\star = 1.26^{+0.42}_{-0.30}$ events per 1000 $M_\odot$ formed (see Appendix C for a discussion on mass-weighted SN rate histories).

However, the parameters which set the shape of the delay time distribution, $\xi$, $\omega$, and $\alpha$, appear very much less constrained by the MCMC. There is a clear maximum at $\omega \approx 60$ that is also highly degenerate with the value of $\xi$. And there does not appear to be any convergence or preference in the value of $\alpha$. While it would appear there is no specific solution to the function preferred by the data, the resultant range in parameters indicate a family of solutions that are indeed related. Characterized by highly negative locations and broad widths, the only part of the distributions (in the 99% confidence interval) which lie in the positive-time domain are the exponential-like tails, as is shown in the inset of Figure 5, a point to be further discussed in Section 4.

## 3. DELAY TIME DISTRIBUTIONS FROM STAR FORMATION HISTORIES

Maoz et al. (2011) detailed a prescription for recovering delay-time distributions from an analysis of the star-formation histories of individual galaxies, both those which host SNe Ia and those that do not, in the duration of a continuous survey. Here, we present an evaluation of the maximum likelihood delay time distribution following the same approach, but performed on the GOODS/CANDELS SN Ia hosts and other field galaxies.

For this analysis we use the star formation histories (SFHs) for galaxies in the GOODS/CANDELS survey area, derived using the Bayesian modeling approach of Pacifici et al. (2012). In summary, the galaxy physical properties are retrieved from a combined analysis of stellar and nebular emission utilizing an extensive library of star formation and chemical enrichment histories. These libraries build a large repository of rest-frame galaxy spectral energy distributions, which are then used to determine likelihood distributions of physical parameters from a Bayesian analysis of observed spectral energy distributions. This method has been applied to the HST/WFC3-F160W-selected CANDELS catalogs for the GOODS-South (Guo et al. 2013), and the GOODS-North (Barro et al. 2019), into SFH catalogs (see Pacifici et al. 2016). For simplicity in this analysis, we adopt only the median derived SFH of each galaxy.

For a given galaxy, the rate history of SNe Ia per year $(r_i)$ would be expressed as:

$$r_i(t) = h^2 \, k \, \varepsilon \int_0^t \Psi_i(t') \, \Phi(t - t') \, dt', \tag{8}$$

where $\Psi_i$ is the SFH of the galaxy (mapped in look-forward time), and $\Phi$ is the global DTD model, also in look-forward time. The product of the rate at the observed epoch $(r_i)$ and the observed control time $(t'_{c,i})$ for the galaxy– which contains all the information on the temporal sampling and depth of the survey– give the expected number of observed SN Ia events $(m_i)$ over the duration of the survey, by

$$m_i = r_i \, t'_{c,i}. \tag{9}$$

The probability distribution for those observed events is likely Poisson, where the likelihood of catching $n_i$ SNe Ia from a galaxy when $m_i$ are expected is

$$P(n_i | m_i) = \frac{m_i^{n_i} e^{-m_i}}{n_i!}. \tag{10}$$

The product of probabilities for all galaxies in the survey would then serve as the likelihood of a given rate model, tuned by the chosen DTD model. The log-likelihood, which is convenient for MCMCs, is then expressed by:

$$L = \prod_i^N P(n_i | M_i) \Rightarrow \ln L = -\sum^N m_i + \sum^N \ln\left(\frac{m_i^{n_i}}{n_i!}\right) \tag{11}$$

in which the last term is zero for the galaxies which did not host SNe Ia during the survey.

Using the control times derived for each survey field using the methods described in Strolger et al. (2015), Figure 6 shows examples "SN Ia rate history" one would derive from Equation 8 using the median-value model from the MCMC on CSFHs done in the previous section. The figure shows star-formation histories for two SN Ia host galaxies, for SN 2002hp and SN 2003dy, respectively (see Strolger et al. 2004, for further details on these events). Both galaxies
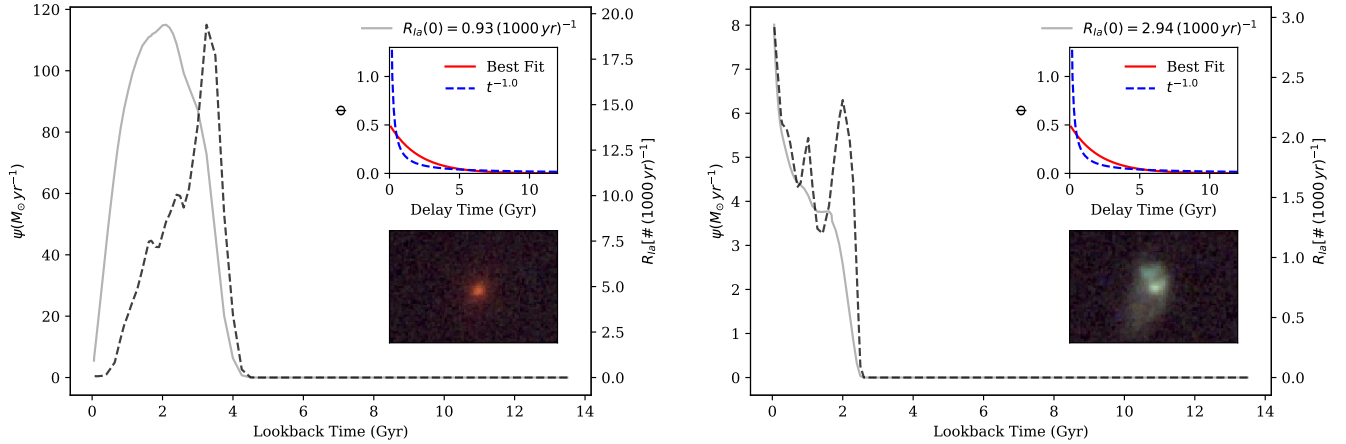
**Figure 6.** Example star formation histories (dashed-line and left ordinate), and the resultant SN Ia rate histories (dotted-line and right ordinate) for two SN Ia host galaxies in our sample, SNe 2002hp (left) and 2003dy (right), in the GOODS-South and GOODS-North fields, respectively. Insets show the delay time distribution applied (upper right, in red) compared to $t^{-1}$ (blue dashed), and a three-color HST ACS/WFC image (lower right) of the SN host galaxy.

are at $z \approx 1.3$, and in the GOODS-South and GOODS-North fields, respectively. The host of SN 2002hp is a fast-forming/slow-quenching passive galaxy that underwent a very large burst of star formation just a few Gyr ago. When that SFH is convolved with the DTD, it results in a relatively large expected rate of 0.93 SNe Ia per millennium at the observed epoch. Conversely, the host of SN 2003dy is actively star forming at the observed epoch, albeit at a more modest rate, and has been active over the last few Gyr. The convolved result is a SN Ia rate about three times larger than the host of SN 2002hp, 2.94 events per millennium at the observed epoch. Nearly all non-hosts have predicted SN Ia rates at their respective observed epochs several orders of magnitude smaller than these two example hosts with this assumed $\Phi(t)$.

The SFH catalog contains 70,375 galaxies in the GOODS-North and South fields, selected with $H < 26$ mag (AB). There are 34 events classified as SNe Ia in the GOODS-South field, and 39 in the North field (Strolger et al. 2004; Dahlen et al. 2008; Rodney et al. 2014), all but 6 of which were matched to host galaxies in the SFH catalog. Two of these hosts were rejected as their events spectroscopic redshifts were very inconsistent with the SFH catalog redshifts, and the other 4 were simply not matched to galaxies in the SFH catalog, as they were either too faint or too near the field edge to be listed in the composite photometry catalogs. Cumulative distribution functions for the total masses and star formation rates (in the observed epoch) of the SN Ia hosts relative to the population of catalog galaxies are shown in Figure 7. Two-sided KS tests on the CDFs by mass and star formation rates do not reject the null hypothesis to $> 95\%$ and $> 99\%$, respectively, implying the population of SN Ia hosts are statistically consistent with the rest of the catalog.

The model parameters, $\xi$, $\omega$, and $\alpha$ were then explored via `emcee.py` in a method similar to what was done in Section 2.5. We keep the same uniform priors as bounds, except we fix $\varepsilon = 0.06$, as it is well constrained in the CSFH MCMC, and setting it as a fixed parameter has the convenience of greatly reducing the computation time. We then set 100 walkers exploring 500 steps on these parameters, the first 50 of which are discarded as burn-in. The maximum likelihood results for the 45,000 iterations on SFHs are identical to the results for the CSFH assessment presented in Section 2.5, as is shown in Table 3. The MCMC likelihood distributions are presented in the Appendix B.

## 4. DISCUSSION

The results of the analyses in Sections 2 and 3 point to a family of delay-time distribution models that are essentially exponential in shape, having fewer prompt events in the 40 Myr to 1 Gyr range than are expected in the $> 1$ Gyr range. These model shapes are generally inconsistent with the results from SD binary population synthesis models, as is shown in Figure 8. They also seem consistent with DD binary population synthesis models, with the caveat that the exponential functional form of our model has difficulty reproducing the distributions that are inherently power-law, as previously indicated. Yet, despite this analytical limitation, it is worth further exploring the comparison in
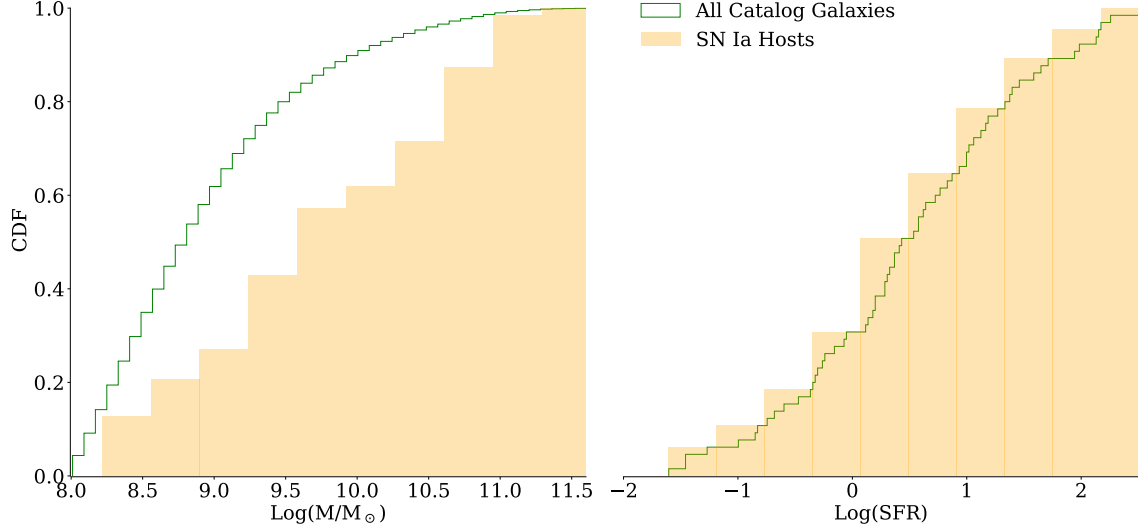
**Figure 7.** CDFs for the total masses (left) and star formation rates (SFR; right) for the 66 SN Ia hosts (yellow), compared to the 70,375 catalog galaxies (green). KS tests on each suggest the population of SN Ia hosts are statistically consistent (to the $> 95\%$ and $> 99\%$ level, respectively) with the rest of the catalog.

the exponential result from this analysis with the assumed power-law distributions that are generally in favor by the community.

Figure 9 shows the DTDs recovered in various time bins from SFH analyses of the Magellanic Clouds (Maoz & Badenes 2010), of Sloan galaxy data (Maoz et al. 2010, 2011, 2012; Graur & Maoz 2013), and from high$-z$ cluster rates (Friedmann & Maoz 2018), along with the derived slopes for power-law models for SN Ia hosts in field ($\beta = -1.1^{+0.08}_{-0.07}$) and galaxy cluster ($\beta = -1.4^{+0.32}_{-0.05}$) environments. Also shown are the exponential best fit models from our analysis, overplotted on the field and cluster data. As a relative goodness-of-fit test, we find $\chi^2_\nu = 0.21$ for cluster hosts ($\nu = 10$) relative to $\beta = -1.3$, $\chi^2_\nu = 3.4$ for field hosts ($\nu = 6$, excluding the LMC+SMC upper limit) relative to $\beta = -1.1$, and $\chi^2_\nu = 2.1$ ($\nu = 17$) for all data compared to our best fit model (also excluding the LMC+SMC upper limit). It appears our exponential model is just as good as, if not better than, the power-law models at describing these recovered delay-time measurements, and has the added benefit of not having to invoke different slopes (or presumably different progenitor channels) for field and clustered SN Ia host environments.

Another common method to testing progenitor models is by comparing the measured rate of SNe Ia in high specific star formation rate (sSFR)[2] galaxies to that in their low-sSFR counterparts, in the modern 'A+B'-model tests (Scannapieco & Bildsten 2005; Andersen & Hjorth 2018). While this grossly addresses the promptness of some fraction of SNe Ia, the test is inherently flawed as it incorrectly assumes the observed SN Ia rate is directly tied to the (A) total mass and (B) the current rate of star formation in a host galaxy, rather than appropriately connecting that SN rate to some past epoch of star formation. That, and the large uncertainties in SN rates that result from complex star-formation rate histories, are the largest sources of error in these tests.

Using the methods described in Section 3 to convolve, for each SN Ia host, the recovered SFH by the best derived DTD to get the SN rate at the observed epoch, and using catalog SFR and total masses at the observed epoch, we derive a track (and associated uncertainty region) in which SNe Ia should lie in specific SN rates (sSNR) as a function of sSFR, as shown in Figure 10. This method is similar to, but inherently more direct than that done in Graur et al. (2015), where in the latter the SFHs are estimated by an exponential law, following Gallazzi et al. (2005) and Kauffmann et al. (2003), and the references therein. This is shown in comparison to measurements from Mannucci et al. (2005), Sullivan et al. (2006), and Smith et al. (2012), and in comparison to tracks expected from $\beta \approx -1.1$ power-law delay time models, and a piecewise model from Andersen & Hjorth (2018). The measurements are consistent with all three tracks over the region in which we have been able to measure them, for star-forming and 'burst' galaxies.

---

[2] Star-formation rate over the total stellar mass at the observed epoch.
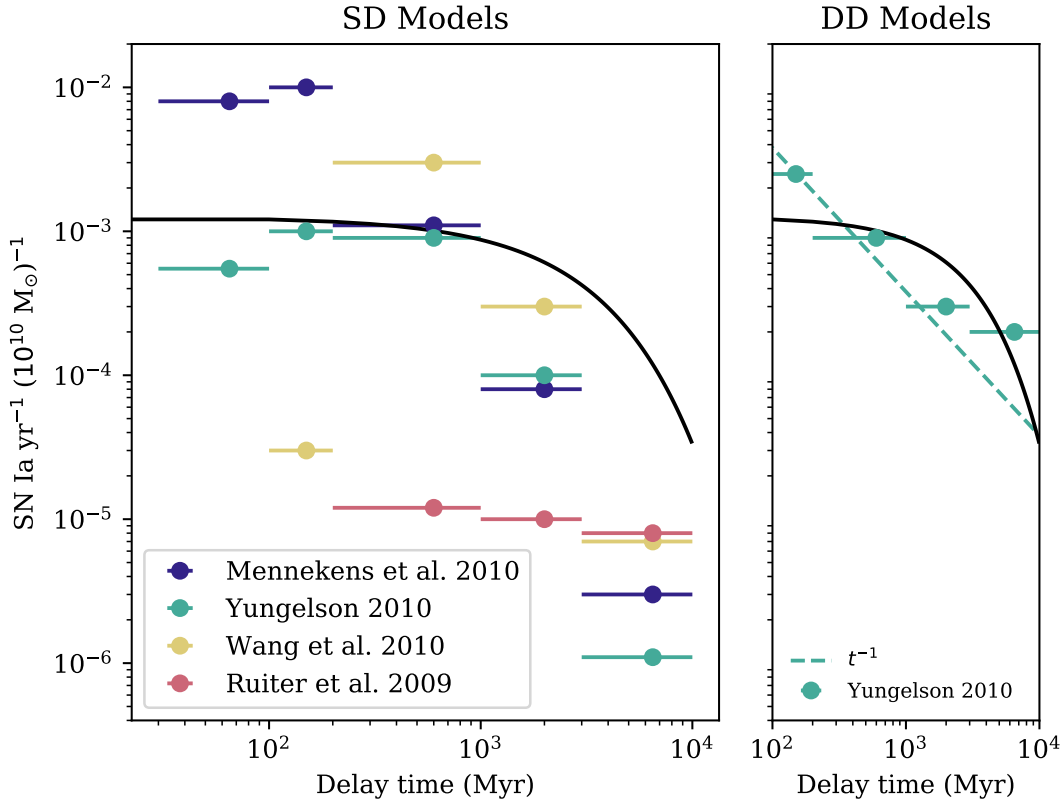
**Figure 8.** Similar to Figure 3, but showing the maximum likelihood model fit.

However, the tracks strongly diverge in the region of passive galaxies, where sSFR $\approx 0$, where there is generally only upper limits to constrain measurements. It is expected that further studies in passive galaxies will provide some clarity. Additionally, tests of these tracks in field dwarf galaxies, specifically those not associated with clusters of galaxies, may be illuminating as they are simpler to model by virtue of having many fewer episodes of star formation.

As a final note, now that the evidence for double white dwarf mergers as the primary source of SNe Ia reaches concordance, it is increasingly interesting to further investigate the fine details of the exact progenitor mechanism.

Delay time distribution reconstructions may finally be able to determine whether conservation of orbital energy is strictly dominant driver (the $\alpha\alpha$-model), as is the case for the common envelope path where both progenitors stars are stripped of their hydrogen envelopes, or if conservation of angular momentum plays a role for most WD/WD mergers initially (the $\gamma\alpha$-model), as it would be in a period of stable mass transfer or in a 'formation reversal' evolutionary track (Toonen & Nelemans 2013). Figure 11 shows the SN Ia rate implied from a binary merger rate as a function of delay time for the $\alpha\alpha$-model and $\gamma\alpha$-model of Toonen et al. (2013), assuming an initial metallicity of $z = 0.02$. Also shown are the delay time distributions from the exponential model from this analysis, and the $\beta = -1$ power-law distributions.

There is striking agreement between the power-law DTD and the $\gamma\alpha$-model (with an appropriate scaling), yet the exponential DTD is more similar to the $\alpha\alpha$-model at large ($> 2$ Gyr) delay times. While the implications of these similarities are unclear at this time, it is clear that further refinement of the rate analysis (through improved rate measures) would be fruitful. Similarly, further refinement of the roles of orbital energy and angular momentum conservation in the modeling may be warranted.
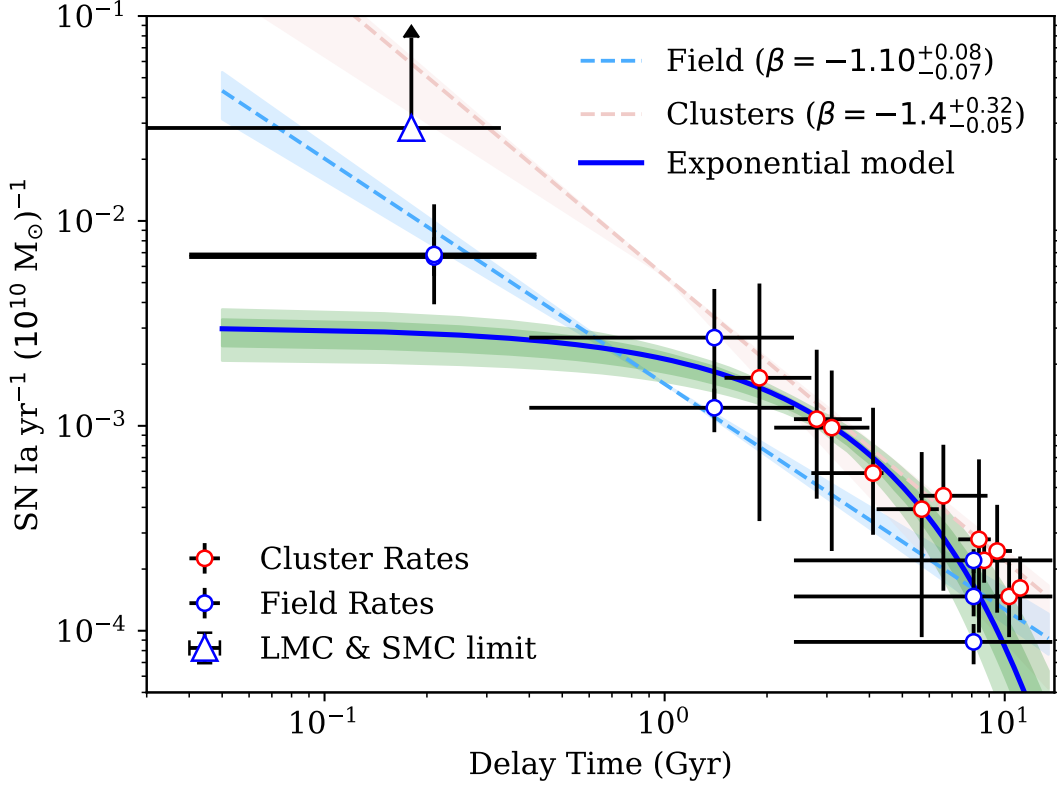
## 5. SUMMARY

**Figure 9.** Reconstructed delay time distributions from various authors, in the LMC & SMC, and in field and galaxy cluster environments. Shown also are the power-law model fits, and associated error regions, for field (in light blue) and cluster (in red) environments. Overplotted is the exponential DTD model (solid blue line) and error region (in green) derived from the analysis in Sections 2 and 3.

We have presented an analysis of type Ia supernova delay time distributions using these two independent methods, from a comparison of volumetric rates to cosmic star formation histories, and through a maximum likelihood method of host star formation histories and their resultant SN Ia yields. From this analysis we can conclude the following:

- Volumetric rate measures at or near the same redshift are reasonably consistent with one another, to within the statistical errors, which are likely underestimated by $7 - 9\%$.

- Assuming $k$ based on analytical arguments, $\varepsilon$ is fairly well constrained at $6.0 \pm 0.3\%$. This is nearly half the expected value from WD binaries (Maoz & Hallakoun 2017). The combination $k \times \varepsilon$ yields $N/M_\star = 1.3^{+0.4}_{-0.3}$ events per 1000 $M_\odot$.

- Family of solutions for the analytical reconstruction of the delay time distribution from volumetric SN Ia rates indicate an exponential-like distribution that is somewhat similar to the $\beta \approx -1$ power-law distributions expected from DD progenitor scenarios, and inconsistent with many SD-model expectations from binary population synthesis.

- DTD solutions from host SFHs following the Maoz et al. (2011) method are identical to those from volumetric rates.

- Exponential solutions are as consistent with empirically recovered delay times as power-law solutions, without having to invoke more than one power-law slope for clustered and field environments.

- Exponential delay-time distributions may yield more consistent results in regards to specific SN Ia rates as a function of their hosts' specific star formation.
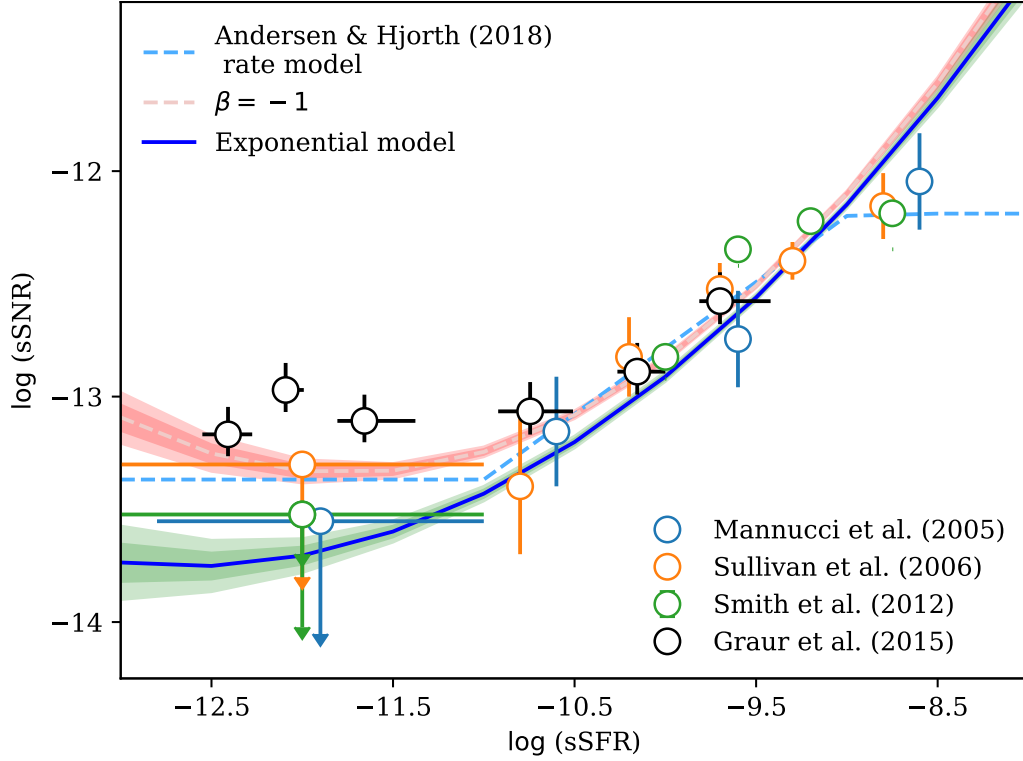
**Figure 10.** Measurements of the specific SN Ia rate relative to specific star formation rates of their hosts, from various authors. Also shown are the expected track (and associated error region) for SNe Ia from this analysis (blue/green region), from $\beta \approx -1.1$ power-law DTDs (in red), and a piecewise model (Andersen & Hjorth 2018, blue-dashed line).
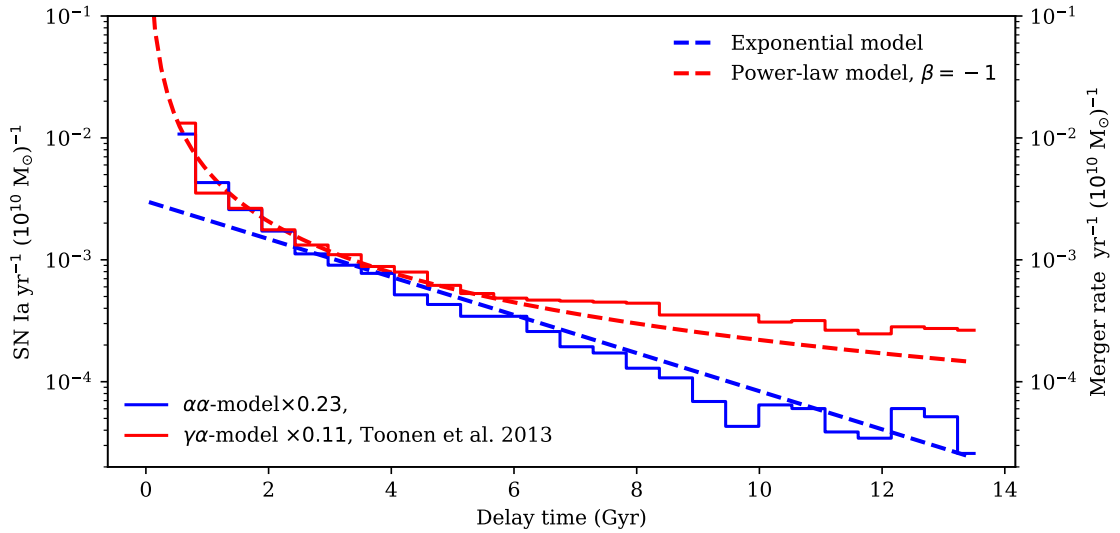


**Figure 11.** DTDs from this analysis (blue dashed) and $\beta = 1$ power-law (red dashed). Also show are the SN Ia rates as a function of delay time implied from different scenarios for WD/WD binary mergers (see Toonen et al. 2013), scaled to match the model lines.

REFERENCES

Andersen, P., & Hjorth, J. 2018, MNRAS, 480, 68, doi: 10.1093/mnras/sty1837

Arnett, W. D. 1969, Ap&SS, 5, 180, doi: 10.1007/BF00650291

Barro, G., Pérez-González, P. G., Cava, A., et al. 2019, ApJS, 243, 22, doi: 10.3847/1538-4365/ab23f2

Blanc, G., Afonso, C., Alard, C., et al. 2004, A&A, 423, 881, doi: 10.1051/0004-6361:20035948

Botticella, M. T., Riello, M., Cappellaro, E., et al. 2008, A&A, 479, 49

Bouwens, R. J., Illingworth, G. D., Oesch, P. A., et al. 2015, ApJ, 803, 34, doi: 10.1088/0004-637X/803/1/34

Brandt, T. D., Tojeiro, R., Aubourg, É., et al. 2010, AJ, 140, 804, doi: 10.1088/0004-6256/140/3/804

Breedt, E., Steeghs, D., Marsh, T. R., et al. 2017, MNRAS, 468, 2910, doi: 10.1093/mnras/stx430

Cappellaro, E., Evans, R., & Turatto, M. 1999, A&A, 351, 459

Cappellaro, E., Turatto, M., Benetti, S., et al. 1993, A&A, 273, 383+

Cappellaro, E., Botticella, M. T., Pignata, G., et al. 2015, A&A, 584, A62, doi: 10.1051/0004-6361/201526712

Catalán, S., Isern, J., García-Berro, E., & Ribas, I. 2008, MNRAS, 387, 1693, doi: 10.1111/j.1365-2966.2008.13356.x

Chen, M. C., Herwig, F., Denissenkov, P. A., & Paxton, B. 2014, Monthly Notices of the Royal Astronomical Society, 440, 1274, doi: 10.1093/mnras/stu108

Croton, D. J. 2013, Publications of the Astronomical Society of Australia, 30, e052, doi: 10.1017/pasa.2013.31

Cummings, J. D., Kalirai, J. S., Tremblay, P.-E., Ramirez-Ruiz, E., & Choi, J. 2018, ArXiv e-prints. https://arxiv.org/abs/1809.01673

Dahlen, T., Strolger, L.-G., & Riess, A. G. 2008, ApJ, 681, 462, doi: 10.1086/587978

Denissenkov, P. A., Truran, J. W., Herwig, F., et al. 2015, Monthly Notices of the Royal Astronomical Society, 447, 2696, doi: 10.1093/mnras/stu2589

Dilday, B., Smith, M., Bassett, B., et al. 2010, ApJ, 713, 1026, doi: 10.1088/0004-637X/713/2/1026

Driver, S. P., Andrews, S. K., da Cunha, E., et al. 2018, MNRAS, 475, 2891, doi: 10.1093/mnras/stx2728

Finkelstein, S. L., Ryan, Jr., R. E., Papovich, C., et al. 2014, ArXiv e-prints. https://arxiv.org/abs/1410.5439

Foreman-Mackey, D., Hogg, D. W., Lang, D., & Goodman, J. 2013, PASP, 125, 306, doi: 10.1086/670067

Friedmann, M., & Maoz, D. 2018, MNRAS, 479, 3563, doi: 10.1093/mnras/sty1664

Gallazzi, A., Charlot, S., Brinchmann, J., White, S. D. M., & Tremonti, C. A. 2005, MNRAS, 362, 41, doi: 10.1111/j.1365-2966.2005.09321.x

Graur, O., Bianco, F. B., & Modjaz, M. 2015, MNRAS, 450, 905, doi: 10.1093/mnras/stv713

Graur, O., & Maoz, D. 2013, MNRAS, 689, doi: 10.1093/mnras/sts718

Graur, O., Poznanski, D., Maoz, D., et al. 2011, MNRAS, 417, 916, doi: 10.1111/j.1365-2966.2011.19287.x

Graur, O., Rodney, S. A., Maoz, D., et al. 2014, ApJ, 783, 28, doi: 10.1088/0004-637X/783/1/28

Guo, Y., Ferguson, H. C., Giavalisco, M., et al. 2013, The Astrophysical Journal Supplement Series, 207, 24, doi: 10.1088/0067-0049/207/2/24

Hinton, S. R. 2016, The Journal of Open Source Software, 1, 00045, doi: 10.21105/joss.00045

Hogg, D. W., Bovy, J., & Lang, D. 2010, ArXiv e-prints. https://arxiv.org/abs/1008.4686

Horesh, A., Poznanski, D., Ofek, E. O., & Maoz, D. 2008, MNRAS, 389, 1871, doi: 10.1111/j.1365-2966.2008.13697.x

Hounsell, R., Scolnic, D., Foley, R. J., et al. 2018, ApJ, 867, 23, doi: 10.3847/1538-4357/aac08b

Iben, Jr., I., & Tutukov, A. V. 1984, ApJS, 54, 335, doi: 10.1086/190932

Kauffmann, G., Heckman, T. M., White, S. D. M., et al. 2003, MNRAS, 341, 33, doi: 10.1046/j.1365-8711.2003.06291.x

Kessler, R., Narayan, G., Avelino, A., et al. 2019, PASP, 131, 094501, doi: 10.1088/1538-3873/ab26f1

Khusanova, Y., Fèvre, O. L., Cassata, P., et al. 2019, arXiv e-prints, arXiv:1903.01884. https://arxiv.org/abs/1903.01884

Kroupa, P. 2001, MNRAS, 322, 231, doi: 10.1046/j.1365-8711.2001.04022.x

Li, W., Chornock, R., Leaman, J., et al. 2011, MNRAS, 412, 1473, doi: 10.1111/j.1365-2966.2011.18162.x

Madau, P., & Dickinson, M. 2014, ARA&A, 52, 415, doi: 10.1146/annurev-astro-081811-125615

Madgwick, D. S., Hewett, P. C., Mortlock, D. J., & Wang, L. 2003, ApJL, 599, L33, doi: 10.1086/381081

Mannucci, F., Della Valle, M., Panagia, N., et al. 2005, A&A, 433, 807, doi: 10.1051/0004-6361:20041411

Maoz, D., & Badenes, C. 2010, MNRAS, 407, 1314, doi: 10.1111/j.1365-2966.2010.16988.x

Maoz, D., & Graur, O. 2017, ApJ, 848, 25, doi: 10.3847/1538-4357/aa8b6e

Maoz, D., & Hallakoun, N. 2017, MNRAS, 467, 1414, doi: 10.1093/mnras/stx102

Maoz, D., & Mannucci, F. 2012, PASA, 29, 447, doi: 10.1071/AS11052

Maoz, D., Mannucci, F., & Brandt, T. D. 2012, MNRAS, 426, 3282, doi: 10.1111/j.1365-2966.2012.21871.x

Maoz, D., Mannucci, F., Li, W., et al. 2011, MNRAS, 412, 1508, doi: 10.1111/j.1365-2966.2010.16808.x

Maoz, D., Mannucci, F., & Nelemans, G. 2014, ARA&A, 52, 107, doi: 10.1146/annurev-astro-082812-141031

Maoz, D., Sharon, K., & Gal-Yam, A. 2010, ApJ, 722, 1879, doi: 10.1088/0004-637X/722/2/1879

Napiwotzki, R., Karl, C. A., Nelemans, G., et al. 2007, in Astronomical Society of the Pacific Conference Series, Vol. 372, 15th European Workshop on White Dwarfs, ed. R. Napiwotzki & M. R. Burleigh, 387. http://adsabs.harvard.edu/abs/2007ASPC..372..387N

Napiwotzki, R., Karl, C. A., Lisker, T., et al. 2019, arXiv e-prints, arXiv:1906.10977. https://arxiv.org/abs/1906.10977

Neill, J. D., Sullivan, M., Balam, D., et al. 2006, AJ, 132, 1126, doi: 10.1086/505532

Nelemans, G., Portegies Zwart, S. F., Verbunt, F., & Yungelson, L. R. 2001a, A&A, 368, 939, doi: 10.1051/0004-6361:20010049

Nelemans, G., Toonen, S., & Bours, M. 2013, in IAU Symposium, Vol. 281, IAU Symposium, 225–231

Nelemans, G., Yungelson, L. R., Portegies Zwart, S. F., & Verbunt, F. 2001b, A&A, 365, 491, doi: 10.1051/0004-6361:20000147

Nomoto, K. 1982, ApJ, 253, 798, doi: 10.1086/159682

Okumura, J. E., Ihara, Y., Doi, M., et al. 2014, ArXiv e-prints. https://arxiv.org/abs/1401.7701

Öpik, E. 1924, Publications of the Tartu Astrofizica Observatory, 25, 1

Pacifici, C., Charlot, S., Blaizot, J., & Brinchmann, J. 2012, MNRAS, 421, 2002, doi: 10.1111/j.1365-2966.2012.20431.x

Pacifici, C., Kassin, S. A., Weiner, B. J., et al. 2016, ApJ, 832, 79, doi: 10.3847/0004-637X/832/1/79

Pain, R., Fabbro, S., Sullivan, M., et al. 2002, ApJ, 577, 120

Pakmor, R., Kromer, M., Taubenberger, S., & Springel, V. 2013, ApJL, 770, L8, doi: 10.1088/2041-8205/770/1/L8

Perlmutter, S., Aldering, G., Goldhaber, G., et al. 1999, ApJ, 517, 565, doi: http://dx.doi.org/10.1086/307221

Perrett, K., Sullivan, M., Conley, A., et al. 2012, AJ, 144, 59, doi: 10.1088/0004-6256/144/2/59

Riess, A. G., Filippenko, A. V., Challis, P., et al. 1998, AJ, 116, 1009, doi: 10.1086/300499

Rodney, S. A., & Tonry, J. L. 2010, ApJ, 723, 47, doi: 10.1088/0004-637X/723/1/47

Rodney, S. A., Riess, A. G., Strolger, L.-G., et al. 2014, AJ, 148, 13, doi: 10.1088/0004-6256/148/1/13

Salpeter, E. E. 1955, ApJ, 121, 161, doi: 10.1086/145971

Scannapieco, E., & Bildsten, L. 2005, ApJL, 629, L85, doi: 10.1086/452632

Smith, M., Nichol, R. C., Dilday, B., et al. 2012, ApJ, 755, 61, doi: 10.1088/0004-637X/755/1/61

Strolger, L., Dahlen, T., & Riess, A. G. 2010, ApJ, 713, 32, doi: 10.1088/0004-637X/713/1/32

Strolger, L. G. 2003, PhD thesis, University of Michigan

Strolger, L.-G., Riess, A. G., Dahlen, T., et al. 2004, ApJ, 613, 200

Strolger, L.-G., Dahlen, T., Rodney, S. A., et al. 2015, ApJ, 813, 93, doi: 10.1088/0004-637X/813/2/93

Sullivan, M., Le Borgne, D., Pritchet, C. J., et al. 2006, ApJ, 648, 868, doi: 10.1086/506137

Takahashi, K., Yoshida, T., & Umeda, H. 2013, ApJ, 771, 28, doi: 10.1088/0004-637X/771/1/28

Tonry, J. L., Schmidt, B. P., Barris, B., et al. 2003, ApJ, 594, 1, doi: 10.1086/376865

Toonen, S., & Nelemans, G. 2013, A&A, 557, A87, doi: 10.1051/0004-6361/201321753

Toonen, S., Nelemans, G., & Portegies Zwart, S. 2013, in IAU Symposium, Vol. 281, Binary Paths to Type Ia Supernovae Explosions, ed. R. Di Stefano, M. Orio, & M. Moe, 223–224

Wang, B., & Han, Z. 2012, NewAR, 56, 122, doi: 10.1016/j.newar.2012.04.001

Webbink, R. F. 1984, ApJ, 277, 355, doi: 10.1086/161701

Whelan, J., & Iben, I. J. 1973, ApJ, 186, 1007, doi: 10.1086/152565

APPENDIX

A. TYPE IA SUPERNOVA RATE MEASURES

Table A lists the volumetric SN Ia rate measurements, from various authors, used in the analysis presented in this manuscript.

**Table 4**. Volumetric SN Ia Rates Used in this Work

| Redshift | $R_{\mathrm{Ia}}$[a] | Stat. Uncertainty | Sys. Uncertainty | Source |
|---|---|---|---|---|
| 0.01 | 0.28 | $+0.09$ $-0.09$ | $+0.0$ $-0.0$ | Cappellaro et al. (1999) |
| 0.03 | 0.28 | $+0.11$ $-0.11$ | $+0.0$ $-0.0$ | Mannucci et al. (2005) |
| 0.0375 | 0.278 | $+0.112$ $-0.083$ | $+0.015$ $-0.00$ | Dilday et al. (2010) |
| 0.1 | 0.259 | $+0.052$ $-0.044$ | $+0.028$ $-0.001$ | Dilday et al. (2010) |
| 0.10 | 0.32 | $+0.15$ $-0.15$ | $+0.0$ $-0.0$ | Madgwick et al. (2003) |
| 0.10 | 0.55 | $+0.50$ $-0.29$ | $+0.20$ $-0.20$ | Cappellaro et al. (2015) |
| 0.11 | 0.37 | $+0.10$ $-0.10$ | $+0.0$ $-0.0$ | Strolger (2003) |
| 0.13 | 0.20 | $+0.07$ $-0.07$ | $+0.05$ $-0.05$ | Blanc et al. (2004) |
| 0.15 | 0.307 | $+0.038$ $-0.034$ | $+0.035$ $-0.005$ | Dilday et al. (2010) |
| 0.15 | 0.32 | $+0.23$ $-0.23$ | $+0.23$ $-0.06$ | Rodney & Tonry (2010) |
| 0.16 | 0.14 | $+0.09$ $-0.09$ | $+0.06$ $-0.12$ | Perrett et al. (2012) |
| 0.2 | 0.348 | $+0.032$ $-0.030$ | $+0.082$ $-0.007$ | Dilday et al. (2010) |
| 0.20 | 0.20 | $+0.08$ $-0.08$ | $+0.0$ $-0.0$ | Horesh et al. (2008) |
| 0.25 | 0.36 | $+0.60$ $-0.26$ | $+0.12$ $-0.35$ | Rodney et al. (2014) |
| 0.25 | 0.365 | $+0.031$ $-0.028$ | $+0.182$ $-0.012$ | Dilday et al. (2010) |
| 0.25 | 0.39 | $+0.13$ $-0.12$ | $+0.10$ $-0.10$ | Cappellaro et al. (2015) |
| 0.26 | 0.28 | $+0.07$ $-0.07$ | $+0.06$ $-0.07$ | Perrett et al. (2012) |
| 0.30 | 0.34 | $+0.16$ $-0.15$ | $+0.0$ $-0.0$ | Botticella et al. (2008) |
| 0.30 | 0.434 | $+0.037$ $-0.034$ | $+0.396$ $-0.016$ | Dilday et al. (2010) |
| 0.35 | 0.34 | $+0.19$ $-0.19$ | $+0.19$ $-0.03$ | Rodney & Tonry (2010) |
| 0.35 | 0.36 | $+0.06$ $-0.06$ | $+0.05$ $-0.06$ | Perrett et al. (2012) |
| 0.42 | 0.46 | $+0.42$ $-0.32$ | $+0.10$ $-0.13$ | Graur et al. (2014) |
| 0.44 | 0.262 | $+0.229$ $-0.133$ | $+0.059$ $-0.120$ | Okumura et al. (2014) |
| 0.45 | 0.31 | $+0.15$ $-0.15$ | $+0.15$ $-0.04$ | Rodney & Tonry (2010) |
| 0.45 | 0.36 | $+0.06$ $-0.06$ | $+0.04$ $-0.05$ | Perrett et al. (2012) |
| 0.45 | 0.52 | $+0.11$ $-0.13$ | $+0.16$ $-0.16$ | Cappellaro et al. (2015) |
| 0.46 | 0.48 | $+0.17$ $-0.17$ | $+0.0$ $-0.0$ | Tonry et al. (2003) |
| 0.47 | 0.42 | $+0.06$ $-0.06$ | $+0.13$ $-0.09$ | Neill et al. (2006) |
| 0.47 | 0.80 | $+0.37$ $-0.27$ | $+1.66$ $-0.26$ | Dahlen et al. (2008) |
| 0.55 | 0.32 | $+0.14$ $-0.14$ | $+0.14$ $-0.07$ | Rodney & Tonry (2010) |
| 0.55 | 0.48 | $+0.06$ $-0.06$ | $+0.04$ $-0.05$ | Perrett et al. (2012) |
| 0.55 | 0.52 | $+0.10$ $-0.09$ | $+0.0$ $-0.0$ | Pain et al. (2002) |
| 0.65 | 0.48 | $+0.05$ $-0.05$ | $+0.04$ $-0.06$ | Perrett et al. (2012) |
| 0.65 | 0.49 | $+0.17$ $-0.17$ | $+0.17$ $-0.08$ | Rodney & Tonry (2010) |
| 0.65 | 0.69 | $+0.19$ $-0.18$ | $+0.27$ $-0.27$ | Cappellaro et al. (2015) |

*Table 4 continued on next page*

Strolger et al.

**Table 4** *(continued)*

| Redshift | $R_{Ia}$[a] | Stat. Uncertainty | Sys. Uncertainty | Source |
|---|---|---|---|---|
| 0.74 | 0.79 | $+0.33$ $-0.41$ | $+0.0$ $-0.0$ | Graur et al. (2011) |
| 0.75 | 0.51 | $+0.27$ $-0.19$ | $+0.23$ $-0.19$ | Rodney et al. (2014) |
| 0.75 | 0.58 | $+0.06$ $-0.06$ | $+0.05$ $-0.07$ | Perrett et al. (2012) |
| 0.75 | 0.68 | $+0.21$ $-0.21$ | $+0.21$ $-0.14$ | Rodney & Tonry (2010) |
| 0.80 | 0.839 | $+0.230$ $-0.185$ | $+0.060$ $-0.120$ | Okumura et al. (2014) |
| 0.83 | 1.30 | $+0.33$ $-0.27$ | $+0.73$ $-0.51$ | Dahlen et al. (2008) |
| 0.85 | 0.57 | $+0.05$ $-0.05$ | $+0.06$ $-0.07$ | Perrett et al. (2012) |
| 0.85 | 0.78 | $+0.22$ $-0.22$ | $+0.22$ $-0.16$ | Rodney & Tonry (2010) |
| 0.94 | 0.45 | $+0.22$ $-0.19$ | $+0.13$ $-0.06$ | Graur et al. (2014) |
| 0.95 | 0.76 | $+0.25$ $-0.25$ | $+0.25$ $-0.26$ | Rodney & Tonry (2010) |
| 0.95 | 0.77 | $+0.08$ $-0.08$ | $+0.10$ $-0.12$ | Perrett et al. (2012) |
| 1.05 | 0.79 | $+0.28$ $-0.28$ | $+0.28$ $-0.41$ | Rodney & Tonry (2010) |
| 1.1 | 0.74 | $+0.12$ $-0.12$ | $+0.10$ $-0.13$ | Perrett et al. (2012) |
| 1.14 | 0.705 | $+0.239$ $-0.183$ | $+0.102$ $-0.103$ | Okumura et al. (2014) |
| 1.21 | 1.32 | $+0.36$ $-0.29$ | $+0.38$ $-0.32$ | Dahlen et al. (2008) |
| 1.23 | 0.84 | $+0.25$ $-0.28$ | $+0.0$ $-0.0$ | Graur et al. (2011) |
| 1.25 | 0.64 | $+0.31$ $-0.22$ | $+0.34$ $-0.23$ | Rodney et al. (2014) |
| 1.59 | 0.45 | $+0.34$ $-0.22$ | $+0.05$ $-0.09$ | Graur et al. (2014) |
| 1.61 | 0.42 | $+0.39$ $-0.23$ | $+0.19$ $-0.14$ | Dahlen et al. (2008) |
| 1.69 | 1.02 | $+0.54$ $-0.37$ | $+0.0$ $-0.0$ | Graur et al. (2011) |
| 1.75 | 0.72 | $+0.45$ $-0.30$ | $+0.50$ $-0.28$ | Rodney et al. (2014) |
| 2.25 | 0.49 | $+0.95$ $-0.38$ | $+0.45$ $-0.24$ | Rodney et al. (2014) |

[a]In units $10^{-4}$ yr$^{-1}$ Mpc$^{-3}$ $h_{70}^3$

## B. MCMC LIKELIHOOD DISTRIBUTIONS

Shown in Figures 12 and 13 are the MCMC likelihood distributions for the volumetric and individual rates, discussed in Sections 2.5 and 3, respectively. Parameter correlations are shown in Tables 5 and 6.
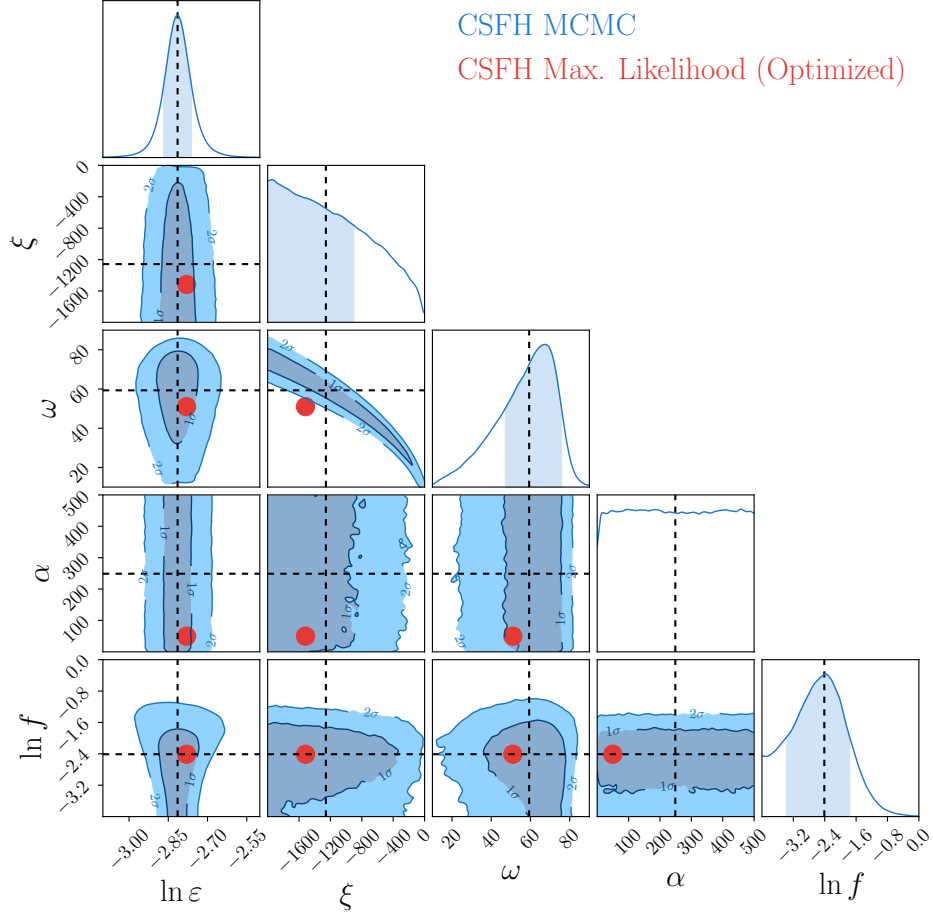
**Figure 12.** MCMC results on the parameters of a unimodal delay-time distribution model, fit to volumetric rate data and CSFH. Dashed lines indicate the median values, and the $1 - \sigma$ and $2 - \sigma$ regions about those best fits are shown in dark and light blue, respectively. The red point marks the maximum likelihood values from the optimized fitting. The plot generated using `ChainConsumer.py` (Hinton 2016).

**Table 5.** MCMC CSFH Parameter Correlations

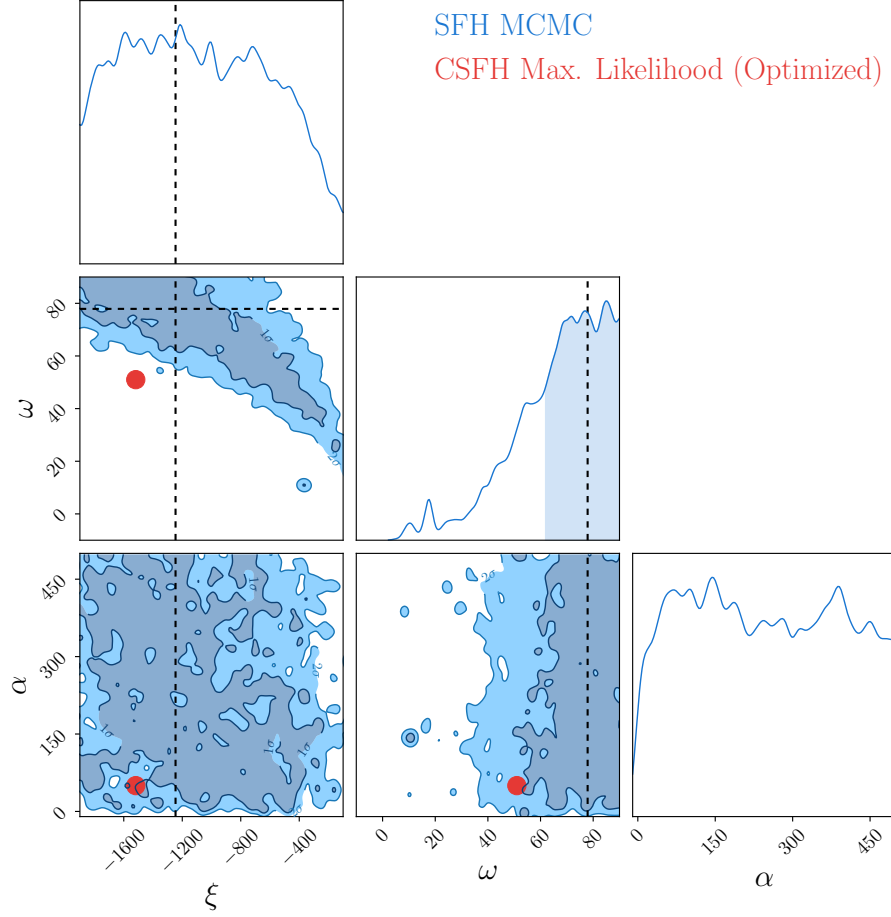|           | $\ln \varepsilon$ | $\xi$ | $\omega$ | $\alpha$ | $\ln f$ |
|-----------|------|-------|-------|-------|-------|
| $\ln \varepsilon$ | 1.00 | 0.00 | 0.02 | 0.00 | -0.02 |
| $\xi$ | 0.00 | 1.00 | -0.95 | 0.01 | 0.02 |
| $\omega$ | 0.02 | -0.95 | 1.00 | -0.01 | -0.05 |
| $\alpha$ | 0.00 | 0.01 | -0.01 | 1.00 | 0.00 |
| $\ln f$ | -0.02 | 0.02 | -0.05 | 0.00 | 1.00 |

**Figure 13.** MCMC results on unimodal delay-time distribution model, fit to SFHs for 70,375 galaxies in the GOODS fields, 67 of which are SN Ia hosts. Dashed lines indicate the maximum likelihood values. The $1 - \sigma$ and $2 - \sigma$ regions about those best fits are shown in dark and light blue, respectively. The red point marks the maximum likelihood values from the optimized fitting. The plot generated using `ChainConsumer.py` (Hinton 2016).

**Table 6.** MCMC SFH Parameter Correlations

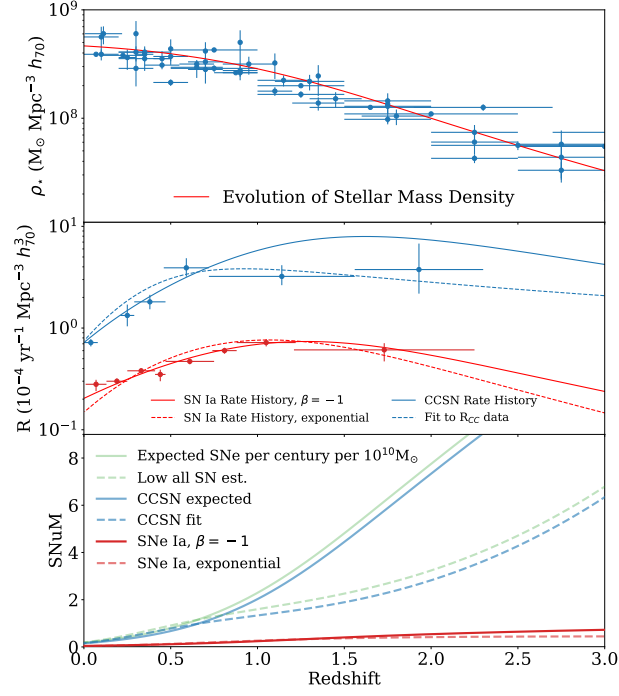|          | $\xi$  | $\omega$ | $\alpha$ |
|----------|--------|----------|----------|
| $\xi$    | 1.00   | -0.76    | -0.18    |
| $\omega$ | -0.76  | 1.00     | 0.14     |
| $\alpha$ | -0.18  | 0.14     | 1.00     |

**Figure 14.** The evolution in mass-weighted SN rates is found by dividing volumetric SN rates by the cosmic evolution of stellar mass density. *Top panel:* the evolution of stellar mass density function in comparison to measures from various authors from the Madau & Dickinson (2014) review. *Middle panel:* volumetric SN rate functions from Strolger et al. (2015) and this manuscript, compared to binned SN rate measures. *Bottom panel:* resultant SNuM($z$) functions.

## C. THE COSMIC MASS-WEIGHTED SUPERNOVA RATE HISTORY

It can be useful to see what volumetric supernova rates imply for the evolution in mass-weighted supernovae rates over cosmic history. Mass-weighted SN rates are often expressed in units of SNuM, or $h^2$ events per century per $10^{10}$ $M_\odot$, and are generally convenient for estimating expected yields from individual galaxies. Using observed volumetric rates, they can be found by

$$\text{SNuM}(z) = \frac{R(z)}{\rho_\star(z)}. \tag{C1}$$

The evolution of the stellar mass density, $\rho_\star(z)$, is found by integrating the cosmic star-formation history over time, expressed by

$$\rho_\star(z) = \rho_A \left(1 - R\right) \int\limits_z^\infty \frac{\dot{\rho}_\star(z')}{H(z')(1 + z')}\, dz', \tag{C2}$$

where

$$H(z) = H_0 \sqrt{\Omega_M(1 + z)^3 + \Omega_\Lambda}, \tag{C3}$$

and $\rho_A = 10^{12}\, M_\odot\, \text{Mpc}^{-3}$. As is shown in Madau & Dickinson (2014), the stellar mass density function of Equation C2 matches well to measures from various surveys when the mass fraction of each generation of stars that is put back in to the ISM is $R = 0.27$.

Figure 14 shows the resultant SNuM($z$) for function by dividing the stellar mass density function into $R_{\text{Ia}}(z)$, for both the $\beta = -1$ power-law and exponential models presented in this paper. Shown also are the results of dividing into the volumetric core-collapse SN rate functions, $R_{\text{cc}}(z)$, from Strolger et al. (2015), assuming either a fit to $R_{\text{CC}}$ data or a model which follows a scaled version of the cosmic star formation history.